

Galaxy formation in WMAP1 and WMAP7 cosmologies

Qi Guo^{1,2,3} \star , Simon White², Raul E. Angulo², Bruno Henriques², Gerard Lemson², Michael Boylan-Kolchin⁴, Peter Thomas⁵, Chris Short⁵

¹ Partner Group of the Max-Planck-Institut für Astrophysik, National Astronomical Observatories, Chinese Academy of Sciences, Beijing, 100012, China

² Max Planck Institut für Astrophysik, Karl-Schwarzschild-Str. 1, 85741 Garching, Germany

³ Institute for Computational Cosmology, Department of Physics, University of Durham, South Road, Durham, DH1 3LE, UK

⁴ Center for Cosmology, Department of Physics and Astronomy, 4129 Reines Hall, University of California, Irvine, CA 92697, USA

⁵ Astronomy Centre, University of Sussex, Falmer, Brighton BN1 9QH

Accepted 2012 October 1. Received 2012 September 25; in original form 2012 May 31

ABSTRACT

Using the technique of Angulo & White (2010) we scale the Millennium and Millennium-II simulations of structure growth in a Λ CDM universe from the cosmological parameters with which they were carried out (based on first-year results from the Wilkinson Microwave Anisotropy Probe, WMAP1) to parameters consistent with the seven-year WMAP data (WMAP7). We implement semi-analytic galaxy formation modelling on both simulations in both cosmologies to investigate how the formation, evolution and clustering of galaxies are predicted to vary with cosmological parameters. The increased matter density Ω_m and decreased linear fluctuation amplitude σ_8 in WMAP7 have compensating effects, so that the abundance and clustering of dark halos are predicted to be very similar to those in WMAP1 for $z \leq 3$. As a result, local galaxy properties can be reproduced equally well in the two cosmologies by slightly altering galaxy formation parameters. The evolution of the galaxy populations is then also similar. In WMAP7, structure forms slightly later. This shifts the peak in cosmic star formation rate to lower redshift, resulting in slightly bluer galaxies at $z = 0$. Nevertheless, the model still predicts more passive low-mass galaxies than are observed. For $r_p < 1$ Mpc, the $z = 0$ clustering of low-mass galaxies is weaker for WMAP7 than for WMAP1 and closer to that observed, but the two cosmologies give very similar results for more massive galaxies and on large scales. At $z > 1$ galaxies are predicted to be more strongly clustered for WMAP7. Differences in galaxy properties, including clustering, in these two cosmologies are rather small out to $z \sim 3$. Given that there are still considerable residual uncertainties in galaxy formation models, it is very difficult to distinguish WMAP1 from WMAP7 through observations of galaxy properties or their evolution.

Key words: cosmology: theory – cosmology: dark matter mass function – galaxies: luminosity function, stellar mass function – galaxies: haloes – cosmology: large-scale structure of Universe

1 INTRODUCTION

In the standard picture, galaxies form through the condensation of gas at the centres of a hierarchically aggregating population of dark matter haloes. The pattern of halo evolution is controlled by the statistics of the primordial density fluctuations which emerged from the early universe, and by the global cosmological parameters which determine their

growth rate at late times. Galaxy evolution depends in addition on the interplay between gas inflows, star formation, radiative, chemical and hydrodynamical feedback, and dynamical processes such as merging and tidal disruption. The intrinsic properties and the spatial distribution of galaxies are thus closely related both to cosmological issues such as the composition and early evolution of the universe, and to astrophysical issues such as the generation and consequences of galactic winds. As a result, the precision with which cosmological conclusions can be drawn from the new generation

\star Email: guoqi@nao.cas.cn

of very large galaxy surveys will depend on the extent to which the relevant signals are distorted by the astrophysics of galaxy formation.

A straightforward approach to exploring how cosmological inferences are limited by our understanding of galaxy formation is to take large-volume, high-resolution simulations of cosmic structure formation in various cosmologies, to populate each with galaxies using a broad variety of physically and observationally consistent treatments of the baryonic processes, and to use mock catalogues to study whether real surveys can distinguish the effects of cosmological and galaxy formation parameters. Direct hydrodynamical simulations do not yet produce galaxy populations with basic statistics (e.g. stellar mass functions) consistent with observation, and are in any case too expensive for even a single simulation to be carried out over a volume approaching those of current surveys. Halo Occupation Distribution (HOD) models can be applied to very large simulations, producing galaxy populations with abundance and correlation statistics in close agreement with observation, but it is unclear whether their simple, purely statistical assumptions lead to physically consistent predictions at different redshifts, or represent adequately the relevant aspects of galaxy formation. Semi-analytic simulations are equally easily constructed and fit galaxy abundances and clustering almost as well as HOD models. Their schematic but plausible representation of formation processes guarantees physically consistent populations at different redshifts, and thus enables direct tests of the influence of individual processes on the large-scale galaxy distribution.

N-body simulations large enough to represent current and next-generation surveys at the resolution required for semi-analytic galaxy formation modelling are still computationally expensive (Angulo & White 2010). As a result, it is not yet feasible to carry out a large suite of simulations scanning the allowed cosmological parameter space. In the current paper, we use the rescaling technique of Angulo & White (2010) to map the Millennium Simulation (MS: Springel et al. 2005) and the Millennium-II Simulation (MS-II: Boyle-Kolchin et al. 2009) from their original WMAP1 cosmology to one with the parameters preferred by the 7-year WMAP results (Komatsu et al. 2011). Our aim is to test whether such scaling, applied to a single simulation, can represent cosmic structure sufficiently accurately to build reliable galaxy catalogues as cosmological parameters are varied throughout the allowed range. We show that the relevant statistical properties of (sub)haloes in the scaled model are indeed very close to those in a simulation carried out directly in the WMAP7 cosmology. Then, we also use such scaling to explore how cosmology affects our predictions for the formation of galaxies.

Our semi-analytic modelling is almost identical to that in Guo et al. (2011)¹. The SAM follows gas infall (both cold and hot, primordial and recycled), shock heating, cooling, star formation, stellar evolution, supernova feedback, black hole growth, AGN feedback, metal enrichment, mergers, and tidal and ram-pressure stripping. Galaxy formation

and evolution are followed from $z > 10$ to the present. As in Wang et al. (2008), who used smaller simulations and an older galaxy formation model, we adjust model parameters independently in each cosmology to reproduce observations of the low-redshift galaxy population, in our case, SDSS stellar mass and luminosity functions, colour distributions, metallicities and gas fractions. We then study differences in the implied clustering and evolution to see if these are clearly related to the difference in cosmological parameters.

Wang et al. (2008) compared results in the WMAP1 and WMAP3 cosmologies. Structure formation differs significantly more between these than between WMAP1 and WMAP7. The most relevant parameters are σ_8 and Ω_m . WMAP3 advocated a much lower $\sigma_8 = 0.7$ and also a lower $\Omega_m = 0.23$ than WMAP1 (0.9 and 0.25, respectively) while WMAP7 prefers an intermediate $\sigma_8 = 0.8$, and a higher $\Omega_m = 0.27$. As a result, structure formation in the WMAP7 cosmology is considerably closer to that in WMAP1 than to that in WMAP3. We will see that, at the current level of precision, predictions for the galaxy populations in WMAP1 and WMAP7 are difficult to distinguish.

This paper is organised as follows. In Sec.2 we briefly describe the MS and MS-II which provide our halo/subhalo merger trees. We compare (sub)halo abundances and clustering as functions of redshift in the two cosmologies, as well as comparing results from the scaled MS to results from a similar simulation carried out directly in the WMAP7 cosmology. This section also describes particularly relevant physical recipes from the galaxy formation model. In Sec.3 we present abundances, scaling relations and clustering properties for low-redshift galaxies in the scaled (WMAP7) simulations and compare them to those in the original unscaled (WMAP1) case. This section also presents a comparison of the evolution of the galaxy populations in the two cosmologies. We summarise our main results and discuss the future application of these techniques in Sec.4. The WMAP7 galaxy catalogues associated with this paper are made publicly available with its acceptance on the same site² and in the same format as the previously released catalogues for the WMAP1 cosmology.

2 N-BODY SIMULATIONS AND SEMI-ANALYTIC MODELS

2.1 N-body simulations

We simulate the evolution of the galaxy population by implementing the galaxy formation model of Guo et al. (2011) on subhalo merger trees extracted from three large cosmological N-body simulations; the Millennium Simulation (MS: Springel et al. 2005), the Millennium-II Simulation (MS-II: Boyle-Kolchin et al. 2009) and a simulation identical to the MS (including the same box-size, $500h^{-1}$ Mpc, output redshift sequence and post-processing pipeline) but with cosmological parameters consistent with the latest observational constraints (MS-W7: Thomas et al., in preparation). In Table 1 we provide the numerical values of the most relevant parameters. All three simulations follow 2160^3 particles from redshift 127 to the present day. The MS and the MS-W7 were

¹ A few minor bugs have been found and corrected since this paper was published, but none of them changes its results significantly.

² <http://www.mpa-garching.mpg.de/millennium>

carried out in a box of side 500 Mpc/h, whereas the MS-II used a box of side 100 Mpc/h. The mass of the simulation particles in these runs is $m_p = 8.61 \times 10^8$ (MS), 6.88×10^6 (MS-II) and $9.31 \times 10^8 M_\odot$ (MS-W7). The MS-W7 was carried out with different fluctuation phases from the MS so that cosmic variance affects any comparison of rare objects between the two simulations.

In addition, we will employ two extra catalogues, with identical cosmological parameters to those of the MS-W7, generated from the MS and MS-II using the scaling algorithm developed by Angulo & White (2010). We will refer to them as MS-SW7 and MSII-SW7, respectively. This algorithm allows scaling of the results of an N-body simulation from its original cosmology to another with modified parameters, and it involves three steps: rescaling the box length, mass and velocity units, relabelling the output times, and rescaling the amplitudes of individual large-scale (linear) fluctuation modes. See Table 1 for the scalings required, and a few examples of the relabelling of outputs. Here we choose $z = 0$ in WMAP7 to correspond to snapshot 53 ($z = 0.28$) in the MS. The scheme reproduces dark halo masses, positions, velocities, and clustering in the target cosmology to the few percent level at all times (Angulo & White 2010; Ruiz et al. 2011). Note that, because of the relabelling, output redshifts other than $z = 0$ do not correspond exactly between the scaled and unscaled simulations. Note also that we do not apply the final step of adjusting the amplitudes of large-scale linear modes, because this has negligible effects on the clustering statistics analysed in this paper.

The most significant difference between the cosmologies preferred by WMAP7 and WMAP1 data, is a 10% lower value of σ_8 . This implies a lower amplitude for primordial density fluctuations, which translates into a decrease in the number of haloes with masses above M_* , and an increase for those below this characteristic mass. The impact of σ_8 was partially compensated by a higher value of Ω_m in WMAP7 compared to WMAP1. As a result, halo mass functions are predicted to be very similar in the two cosmologies at $z = 0$ over the range of halo masses most relevant for galaxy formation. In the next subsection we will explore in more detail how these changes in cosmology affect aspects of dark matter structure relevant for galaxy formation.

2.2 Dark matter halo and subhalo properties

Galaxies form through the condensation of gas and the merging of satellites, both of which are accreted along with the dark matter as their surrounding haloes build up with time. Their stellar mass is thus closely related to the total mass of their haloes. The outer parts of haloes are removed by tidal effects if they fall into larger systems and so become satellite subhaloes, while the stars and gas of their central galaxies are less easily stripped. Thus the stellar mass of satellite galaxies is more closely linked to halo mass at infall than it is to current subhalo mass (see, for example, the galaxy formation simulations of Springel et al. 2001; Gao et al. 2004; Guo et al. 2011). This realisation led to a simplified model which assumes a monotonic relation between the stellar mass or luminosity of a galaxy and the maximum mass or circular velocity ever attained by its halo (e.g. Vale & Ostriker 2004; Conroy et al. 2006; Moster et al. 2010; Guo et al. 2010). This scheme has proved successful

Table 1. Summary of the parameters adopted in our WMAP1 and WMAP7 cosmologies, as well as of the scale factors, f_l , f_{mp} and $f_{m_{vir}}$ for simulation box length, particle mass and halo mass, respectively. Here F is a function of (original) halo concentration parameter c and of the ratio between the (dimensionless) matter density in the WMAP1 cosmology at the output redshift under consideration, $\Omega_o(z_o)$, and that for WMAP7 at the redshift to which this output maps, $\Omega_t(z_t)$. In addition we give the redshifts z_o in WMAP1 which are mapped to redshifts $z_t = 0, \sim 1$ and ~ 3 in WMAP7

| Parameter | WMAP1 | WMAP7 |
|------------------|--------|---|
| Ω_m | 0.25 | 0.272 |
| Ω_Λ | 0.75 | 0.728 |
| Ω_b | 0.0425 | 0.045 |
| h | 0.73 | 0.704 |
| n | 1 | 0.961 |
| σ_8 | 0.9 | 0.807 |
| f_l | 1 | 1.043 |
| f_{mp} | 1 | 1.23488 |
| $f_{m_{vir}}$ | 1 | $f_{mp} \times F(c, \Omega_o(z_o)/\Omega_t(z_t))$ |
| redshift | 0.28 | 0 |
| | 1.39 | 1.02 |
| | 3.58 | 2.92 |

in matching many local galaxy properties, including the Tully-Fisher relation, galaxy correlation functions and the observed stellar mass-halo mass relation. Its assumptions are at least approximately obeyed by more physical models for the formation and evolution of the galaxy population (e.g. Guo et al. 2011)

Fig. 1 shows the abundance of dark matter (sub)haloes as a function of M_{200} , the mass within a sphere centred on the gravitational potential minimum enclosing mean density 200 times the critical value. For central objects, this corresponds to its current value, but for satellites, it corresponds to the value just prior to (last) infall onto the current host. We display results at redshifts 0, 1, 3 and 6. Solid and dashed curves refer to the WMAP7 and WMAP1 cosmologies, respectively, whereas coloured lines indicate our different simulations.

Results from the MS and MS-II converge well over the mass range where both simulations have adequate resolution and good statistics. This range shifts to lower mass at higher redshift as satellites become progressively less important. At $z = 0$ the two simulations agree closely for masses above $10^{12} M_\odot/h$. This is more than an order of magnitude larger than the mass needed to get similar agreement for the standard halo mass function (e.g. Boylan-Kolchin et al. 2009). This reflects the inclusion of subhalos; for the majority of subhalos to be reliably identified after infall and stripping they need to have $\sim 10^3$ particles at infall.

At $z = 6$, (sub)haloes of all masses are more abundant at every mass in WMAP1 than in WMAP7, but by $z = 1$ the two mass functions are very close for $M_{sh} < 10^{12} M_\odot/h$ and at $z = 0$, they overlap for $M_{sh} < 10^{12.5} M_\odot/h$, remaining close at higher masses although there are always more high-mass haloes in WMAP1 than in WMAP7. The relatively small differences between the two cosmologies, especially at low redshift, reflect the fact that the lower value of σ_8 in WMAP7 is largely compensated by its higher value of Ω_m .

A comparison of the blue and red solid curves in Fig. 1

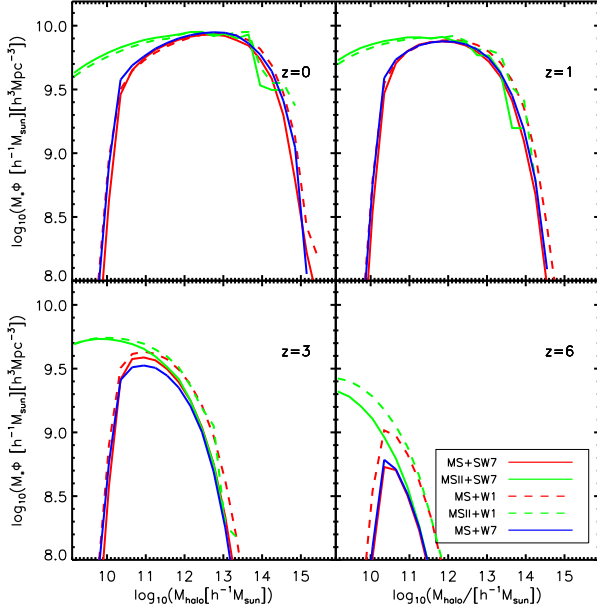


Figure 1. Differential (sub)halo mass functions at $z \approx 0, 1, 3$ and 6 , as indicated by the label in each panel. For the main subhalo of each FoF group this is the current M_{200} of the group, while for satellite subhaloes it is the M_{200} value just prior to first infall. Solid and dashed curves show measurements for the WMAP7 and the WMAP1 cosmology, respectively. Red, green and blue curves are results from the MS, the MS-II and the MS-W7, respectively.

shows that the (sub)halo mass functions for the scaled MS agree very well with those for the MS-W7 (which was carried out directly in the WMAP7 cosmology) over the range not affected by resolution. This confirms the results of Angulo & White (2010) and Ruiz et al. (2011), and extends them to larger simulations and to the (sub)halo mass function, which is the most relevant mass function for modelling of the galaxy population. The differences seen at low masses, most noticeably at $z = 3$, are partly due to fact that output times do not coincide exactly between the two simulations, and partly to different mass resolutions, numerical settings and initial phases. In addition, at these low masses many satellite haloes are artificially lost in a way that depends sensitively on the mass and force resolution of each simulation.

Halo of given mass have higher maximum circular velocity, and hence higher density and virial temperature, at higher redshift. This is important for galaxy formation modelling because of its effect on gas cooling rates. Fig. 2 is directly analogous to Fig. 1, differing only in that (sub)haloes are characterised by their maximum circular velocity rather than by their mass. Again the velocity is taken to be the current value for main subhaloes and the value at infall for satellite subhaloes. The behaviour here is very similar to that in the earlier plot, with good convergence between MS and MS-II and between the MS scaled to the WMAP7 cosmology and the MS-W7.

Fig. 3 shows the fraction of subhaloes that are satellites rather than dominant, “main” subhaloes as a function of $V_{max, infall}$ and redshift. The various curves are colour

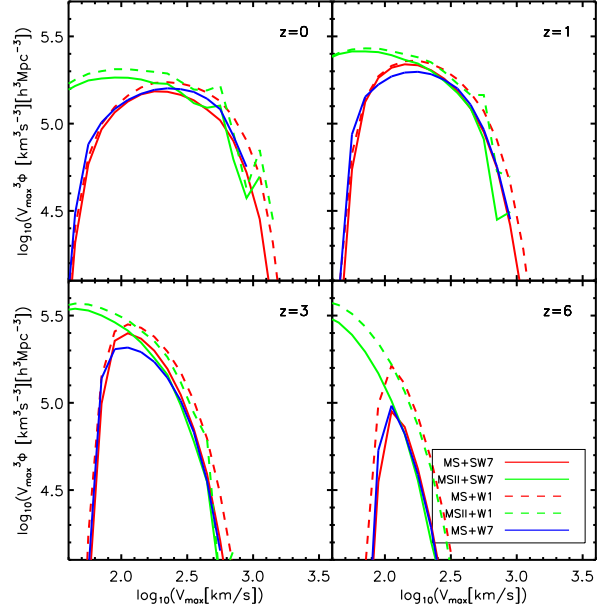


Figure 2. Differential distributions of dark halo $V_{max, infall}$ as a function of redshift. For the main subhalo of each FoF group this is taken to be its current maximum circular velocity, while for satellite subhaloes it is the value at infall. The different panels, line colours and line types correspond exactly to those in Fig. 1.

and line-style coded as in Figures 1 and 2. Not surprisingly, the MS-II, with its 125 times better mass resolution, always finds higher satellite fractions than the MS. The threshold at which the satellite fractions converge is higher than the one where the mass functions and $V_{max, infall}$ functions converge. The satellite fraction increases with decreasing (sub)halo mass, but never exceeds 50%. This fraction is also a decreasing function of redshift. At $z = 6$ the maximum value is only about 10%. Comparing WMAP1 to WMAP7, we find that satellite fractions are always higher in WMAP1 which should be reflected in a (mild) enhancement of satellite galaxy abundance in this cosmology. Once again there is good agreement between the direct simulation of the WMAP7 cosmology (MS-W7, solid blue curves) and the results from the scaled MS simulation (solid red curves), although at $z = 0$, the direct simulation predicts a 4% lower satellite fraction than the rescaled one at $\log V_{max, infall} = 2.25$. This is probably a consequence of the rescaling of the time axis which results in an underestimate of the number of orbital times available for merging in the scaled simulation.

So far we have studied the abundance of satellite and central (sub)haloes as a function of mass and maximum circular velocity. In Fig. 4 we compare their spatial clustering by plotting the two-point correlation function for all (sub)haloes with $V_{max, infall}$ greater than 100 and 200 km/s, where $V_{max, infall}$ is defined as in Fig. 2. The results in this plot are based on the MS, MS-SW7 and MS-W7 only. Although results for the two cosmologies are very similar, the correlation function is slightly higher in WMAP1 than in WMAP7 for both maximum circular velocity limits. This is consistent with the larger bias expected for given halo mass at lower σ_8 , and with the larger satellite fractions

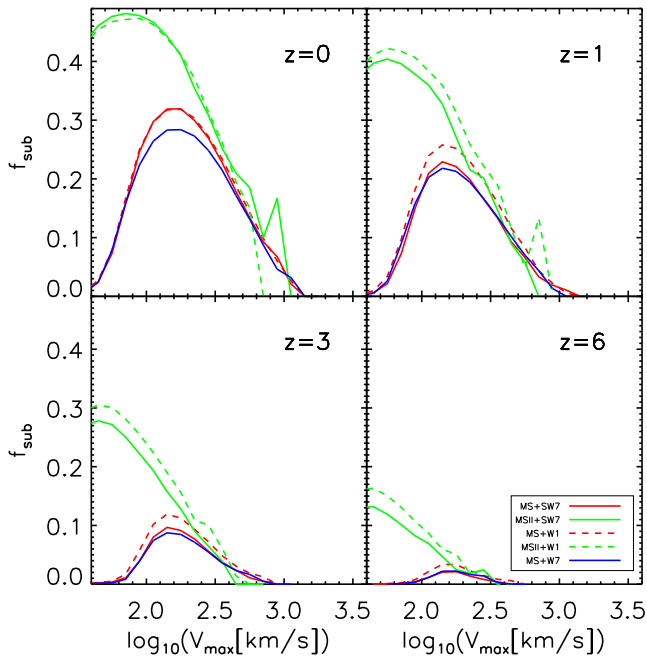


Figure 3. Fraction of satellite subhaloes as a function of $V_{max,infall}$ at $z \approx 0, 1, 3$ and 6. The various curves are colour and line-type coded as in Fig. 1 and 2

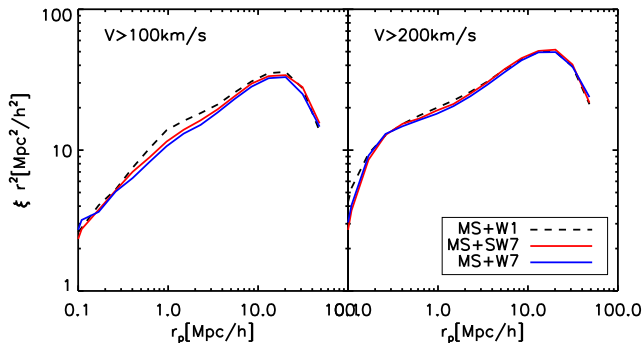


Figure 4. Autocorrelation functions for (sub)haloes with $V_{max,infall} > 100$ (left panel) and 200 km/s (right panel). Solid red curves are for the MS scaled to the WMAP7 cosmology while solid blue curves are for MS-W7. Dashed black curves refer to the original MS in its WMAP1 cosmology.

in WMAP1. Again the results for the MS scaled to the WMAP7 cosmology agree very well with the direct measurements in MS-W7. Given the small size of the differences between the two cosmologies at all redshifts, we can anticipate that galaxy formation models will produce similar galaxy populations in the two cases for similar values of their efficiency parameters. We will explore this in great detail throughout section 3.

2.3 Semi-analytic modelling of galaxy formation

In the standard galaxy formation scenario, gas and dark matter fall together into growing dark haloes, both diffusely and in clumps. The gas then shocks, radiating away its in-

fall energy either immediately or more slowly from a hot quasi-static atmosphere, and settling into a central rotationally supported gas disk. As discussed in the original papers (Rees & Ostriker 1977; White & Rees 1978; White & Frenk 1991) the rapid cooling or “cold flow” regime is dominant at early times and in lower mass haloes, while the cooling flow regime is more important at late times and in massive haloes (see van de Voort et al. (2011) for a recent discussion). When the gas disk is sufficiently massive it starts to form stars, as well as to build a central black hole. The evolving stellar populations then pump energy, mass and heavy elements into their surroundings through stellar winds and supernovae, and the accreting black hole also heats its environment. As satellite galaxies orbit within larger haloes (“clusters”) they are affected by dynamical processes which can strip their remaining gas, can tidally truncate their stellar and dark matter components, and can cause them to merge with the central galaxy, stimulating starbursts and further AGN activity. These cooling and feedback processes regulate the growth of galaxies and shape their mass and luminosity functions.

In this work we use the galaxy formation model of (Guo et al. 2011, hereafter G11) to follow all these baryonic processes within dark matter (sub)halo trees which describe the evolution of nonlinear structure within the MS, the MS-II and the MS-W7. This is the latest version of the simulation-based model of the Munich group (Kauffmann et al. 1999; Springel et al. 2001, 2005; Croton et al. 2006; De Lucia & Blaizot 2007). G11 adjusted model parameters so that galaxy abundances in the MS and MS-II agreed with those measured in the Sloan Digital Sky Survey (SDSS) as a function of stellar mass, luminosity, size, star formation rate, colour, morphology, gas content, metallicity and characteristic velocity. Although they were able to reproduce many observed properties of galaxies both in the local universe and at high redshift (see also, Henriques et al. 2012), G11 highlighted three significant problems. At early times ($z \geq 1$) the abundance of low-mass galaxies is significantly overpredicted. At low redshift, satellite galaxies in groups and clusters are too uniformly red (see also, Weinmann et al. 2011). Finally, low-mass galaxies are too strongly clustered on scales below about 1 Mpc.

These problems may be related: low-redshift, red satellites are the descendants of low-mass galaxies which formed and fell into larger systems at early times, thus increasing small-scale clustering. As we saw above there are fewer massive haloes at high redshift and less substructure at low redshift in the WMAP7 cosmology than in WMAP1. In this paper we therefore apply the G11 galaxy formation model to the WMAP7 cosmology to investigate whether the problems are alleviated. We follow the same philosophy as in the original paper, adjusting the efficiency parameters of the model to fit galaxy abundances in the SDSS as a function of galaxy properties. We then compare the evolution and clustering of galaxies with other data in order to test the model. In particular, in this paper we compare results for the two cosmologies. In the remainder of this subsection, we briefly describe our treatment of the processes for which parameters are readjusted in order to maintain agreement between model predictions and local observations when the cosmology is changed.

In the G11 model, the star formation rate is assumed

to be proportional to the mass excess above threshold of the cold gas disk and inversely proportional to its rotation period:

$$\dot{M}_* = \alpha(M_{\text{gas}} - M_{\text{crit}})/t_{\text{dyn}}, \quad (1)$$

where α is a free parameter describing the star formation efficiency. Recent studies of galaxy-wide star formation suggest $\alpha \sim 0.02$ for present-day disk galaxies, although with a characteristic time which is determined by the atomic-to-molecular transition rather than the disk orbital period (Bigiel et al. 2011). We operationally define the orbital or dynamical time as $t_{\text{dyn}} = 3R_{\text{gas,d}}/V_{\text{max}}$, where $R_{\text{gas,d}}$ is the gas disk scale length and V_{max} is the maximum circular velocity of the (sub)halo. M_{crit} is a critical mass above which stars can form, obtained by integrating the critical surface density assuming a flat rotation curve and a gas velocity dispersion of 6 km/s:

$$M_{\text{crit}} = 11.5 \times 10^9 \left(\frac{V_{\text{max}}}{200 \text{ km/s}} \right) \left(\frac{R_{\text{gas,d}}}{10 \text{ kpc}} \right) M_{\odot}. \quad (2)$$

As stars evolve, 43% of the total mass of each generation is returned to the interstellar medium immediately, a crude approximation to the integrated mass loss which more realistically should be spread out over a period extending to several Gyr. Supernova explosions are also assumed to take place instantaneously, releasing energy to heat surrounding gas, as well as heavy elements to enrich it. The total energy released by supernovae is modelled as

$$\delta E_{\text{SN}} = \epsilon_{\text{halo}} \times \frac{1}{2} \delta M_* V_{\text{SN}}^2. \quad (3)$$

where $0.5V_{\text{SN}}^2$ is the mean kinetic energy of supernova ejecta per unit mass of stars formed. ϵ_{halo} is a halo-dependent efficiency:

$$\epsilon_{\text{halo}} = \eta \times \left[0.5 + \left(\frac{V_{\text{max}}}{V_{\text{eject}}} \right)^{-\beta_1} \right], \quad (4)$$

where η is an adjustable parameter, β_1 describes the dependence on V_{max} , and V_{eject} sets the normalisation. Note that ϵ_{halo} is assumed to saturate at unity, i.e., the total energy reheating/ejecting gas from galaxies cannot exceed the total amount of energy provided by SNe.

Part of this energy is used to reheat gas from the ISM to a hot gas halo:

$$\delta M_{\text{reheat}} = \min[\epsilon_{\text{disk}} \times \delta M_*, 2\delta E_{\text{SN}}/V_{\text{max}}^2]. \quad (5)$$

where δM_* is the mass of newly formed stars and ϵ_{disk} is another halo-dependent efficiency similar to that of Eq. 4,

$$\epsilon_{\text{disk}} = \epsilon \times \left[0.5 + \left(\frac{V_{\text{max}}}{V_{\text{reheat}}} \right)^{-\beta_2} \right]. \quad (6)$$

Here ϵ , β_2 and V_{reheat} are again adjustable parameters. When the first term on the *rhs* of Eq. 5 is the smaller, residual feedback energy is used to eject hot gas out of the halo altogether (see G11).

One of the most frequently invoked mechanisms to quench star formation in the central galaxies of clusters is feedback from a radio AGN. Following Croton et al. (2006), G11 adopt a model in which the heating rate from radio AGN is expressed as

$$\dot{E}_{\text{AGN}} = 0.1c^2 \dot{M}_{\text{BH}}$$

$$= 0.1c^2 \kappa \left(\frac{f_{\text{hot}}}{0.1} \right) \left(\frac{V_{\text{vir}}}{200 \text{ km/s}} \right)^3 \left(\frac{M_{\text{BH}}}{10^8/hM_{\odot}} \right), \quad (7)$$

where, M_{BH} is the mass of the black hole, f_{hot} is the hot gas fraction of the halo, V_{vir} is the circular velocity at R_{200} and κ parametrises the efficiency of hot gas accretion. Massive halos form later in WMAP7 than in WMAP1, so one expects that a lower value of this accretion efficiency will be required if central galaxies are to grow to the same mass as in the WMAP1 cosmology.

In the code module which models the disruption of type 2 galaxies (satellites which have lost their subhaloes) G11 accidentally failed to use updated positions. Effectively, this meant that these objects were either disrupted when they first lost their subhaloes, or not at all. This bug has been fixed in the current version of the code, which now correctly identifies the position of each type 2 in this module (as in the rest of the code) with that of the most bound particle in its subhalo at the last time this was identified, modified by a shrinking factor to account for dynamical friction. This correction results in small differences between the WMAP1 results of this paper and those in G11.

3 RESULTS

In this section, we compare predicted galaxy properties in the WMAP1 and WMAP7 cosmologies. As noted above, we readjust star formation and feedback parameters for the WMAP7 cosmology so that the low-redshift stellar mass function for the scaled MS and MS-II simulations matches that inferred from the SDSS, just as was done for WMAP1 by Guo et al. (2011). The galaxy formation parameters we adopt for the two cosmologies are summarised in Table 2 where they differ. Parameters not listed in this table are held to the values adopted by G11. Note that there are some degeneracies between parameters in these models, so that the sets we use here are not the only ones which can produce fits to the observations of the quality we show.

Overall, fitting the observed stellar mass function in the WMAP7 cosmology requires somewhat lower star formation and feedback efficiencies than in WMAP1. Together with the somewhat later formation of structure, this results in a relatively higher fraction of blue galaxies in the WMAP7 cosmology. The dependence of SN feedback on V_{max} that we adopt in WMAP7 is weaker than in WMAP1, resulting in less efficient ejection by winds from low-mass systems. Since massive structures form later in WMAP7, less efficient AGN feedback is required to allow brightest cluster galaxies to grow to the observed size. We now analyse trends of this kind in more detail.

3.1 Stellar mass and luminosity functions

Fig. 5 compares model stellar mass functions for the WMAP1 (dashed) and WMAP7 (solid) cosmologies to the observational data from Li & White (2009) and Baldry et al. (2008) which we have fitted. Red and green curves refer to the MS and the MS-II, respectively. Our galaxy formation modelling is able to match the observed galaxy abundance equally well in the two cosmologies. Observational stellar mass estimates should differ slightly in our

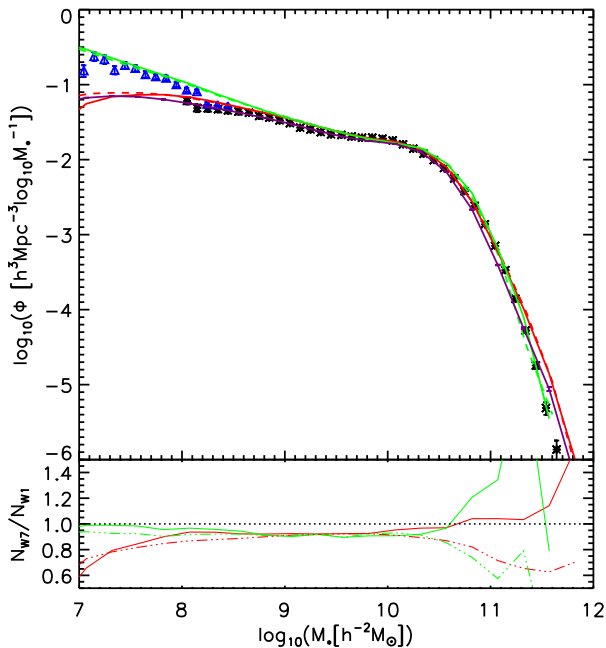


Figure 5. Stellar mass functions predicted by our galaxy formation models. Symbols are the observed SDSS mass functions of Li & White (2009) and Baldry et al. (2008). Red and green curves refer to models implemented on the MS and MS-II, respectively. Solid curves are for the WMAP7 cosmology, while dashed ones are for WMAP1. In the bottom panel, solid lines compare the ratio of the galaxy abundances in these WMAP7 and WMAP1 models as a function of stellar mass; again red is for the MS and green is for the MS-II. The difference is less than 8% except at the very high mass end. This panel also shows as dashed-dotted curves the result of applying the original WMAP1 galaxy formation parameters to the scaled WMAP7 simulations. Even without retuning, the change in cosmology affects the mass function only at about the 10% level (except at the highest masses). Finally, the upper panel also shows the result of applying our WMAP7 galaxy formation model to the MS-W7, a repeat of MS carried out directly in the WMAP7 cosmology (purple curve).

two cosmologies due to the geometry dependence of luminosity distance (we already account for the difference in H). This residual difference is about 0.3% at $z=0.1$ and reaches 3.7% at $z = 1.5$. These effects are small enough that we neglect them in the following.

At masses less than $10^{10.5} M_{\odot}$ the predicted abundances are almost identical in the two cosmologies, as shown by the detailed comparison in the lower panel. At higher masses, the WMAP7 model predicts slightly more galaxies. This reflects the specific AGN feedback efficiency we adopt for this cosmology, which determines the masses of the biggest galaxies. Although we re-tuned the galaxy formation parameters to reproduce the $z = 0$ stellar mass function in the WMAP7 cosmology, the difference in mass function evolution between the two cosmologies is, in fact, sufficiently small that a good fit is obtained even if we do not change these parameters at all. This is illustrated in the lower panel of Fig. 5 where the dashed-dotted curves show the ratio of the mass functions obtained when the WMAP1 galaxy formation model is run on the scaled WMAP7 simulations to those obtained when it is run on the original WMAP1 simulations.

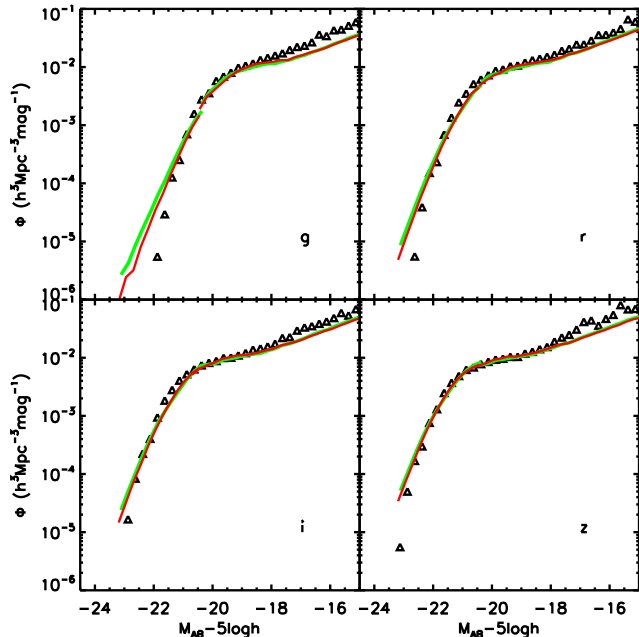


Figure 6. Galaxy luminosity functions in the SDSS g , r , i and z photometric bands. The smooth green and red curves are predictions from our WMAP7 and WMAP1 models, respectively and are taken from the MS at the bright end and from the MS-II at absolute magnitudes below about -20.0 . The symbols are observational data for a low-redshift SDSS sample taken from Blanton et al. (2005).

These mass functions are within 10% of each other except at the highest masses.

To explore how well our rescaling technique works, we have also implemented our WMAP7 galaxy formation model with unchanged parameters on a repeat of the MS carried out directly using the updated WMAP7 cosmology (MS-W7). We overplot the resulting stellar mass function as a purple curve in the upper panel of Fig. 5. The results are very similar, particularly when account is taken of the fact that the effective mass resolution of the scaled MS simulation is poorer by a factor of 1.23 than that of MS-W7, and that the initial phases of the simulations are different so that the abundance comparison is affected by cosmic variance (Smith 2012). The two functions differ primarily through a small offset of up to 0.1dex in stellar mass, with the direct simulation producing systematically slightly lower mass galaxies than the scaled MS. This offset leads to very small abundance differences at stellar masses below that of the Milky Way, but to differences approaching a factor of 2 at the highest masses where cosmic variance is substantial. For the rest of this paper, we will compare the scaled and un-scaled Millennium Simulations in order to be able to test for numerical convergence by comparing MS and MS-II and to avoid cosmic variance effects at high mass.

Fig. 6 shows luminosity functions in the SDSS g , r , i and z bands. Symbols are taken from Blanton et al. (2005); green and red curves are model predictions for the WMAP7 and WMAP1 cosmologies, respectively. We include the h factor in the magnitude and volume units in order to compare the observational data to the different cosmologies in a fair

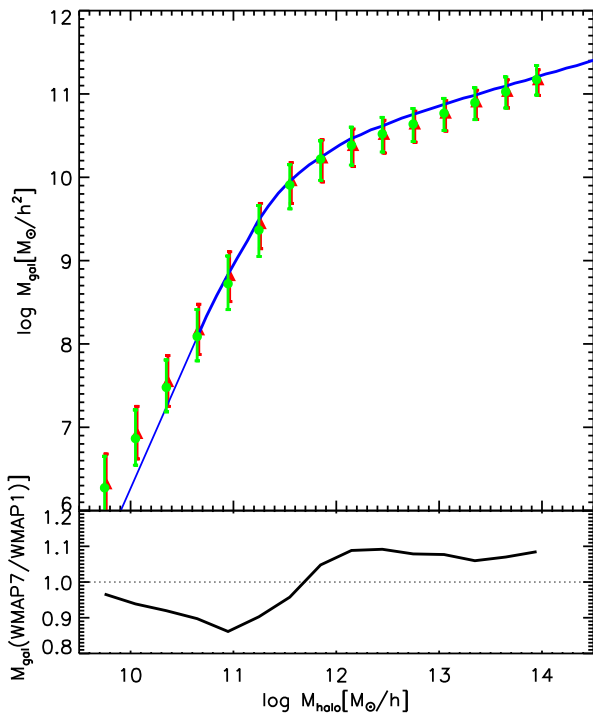


Figure 7. Galaxy stellar mass as a function of maximum past halo mass, as predicted for the WMAP7 (green) and WMAP1 (red) cosmologies. Symbols with error bars represent the median values and the $\pm 1\sigma$ scatter in the models. They are offset slightly in the x -direction for clarity. The blue curve is the WMAP1 relation derived directly from the SDSS stellar mass function and from subhalo abundances in the MS and MS-II under the assumption that the two quantities are monotonically related without scatter (Guo et al. 2010). The lower panel shows the ratio of the central value of the red and green bars.

way. Model predictions are from the MS for galaxies with absolute magnitudes brighter than -20 and from the MS-II for fainter galaxies. For both cosmologies the predictions agree reasonably well with observation in all four bands. In the r band, the predictions are identical in two cosmologies over the full magnitude range. For very bright galaxies, the g -band luminosity function is higher in WMAP7 than in WMAP1 which already overpredicts the observed abundance. As pointed out by G11 this may reflect the inadequacy of our dust model in massive star-bursting galaxies. WMAP7 gives slightly higher results since it predicts slightly more major mergers of gas-rich massive galaxies at low redshift.

3.2 Stellar mass vs. Infall halo mass relation

Galaxies form by the condensation of gas at the centres of dark matter haloes, and as a result there is a relatively tight relation between their stellar masses and the dark matter masses of their haloes. After a galaxy falls into a more massive system, its halo mass can be reduced substantially by tides, while the stellar distribution is much less affected. For such satellites, stellar mass is more closely related to halo mass just before infall than to current halo mass. Thus, many authors have assigned galaxies

to (sub)haloes in dark matter simulations by assuming a monotonic relation between stellar mass and maximum past (sub)halo mass and forcing the simulation to reproduce the observed abundance of galaxies as a function of stellar mass (e.g. Vale & Ostriker 2004; Conroy et al. 2006; Moster et al. 2010; Guo et al. 2010). For a concordance Λ CDM cosmology, the relation obtained through such subhalo abundance matching is consistent with observational estimates from weak lensing and satellite galaxy dynamics, and results in galaxy correlations as a function of stellar mass which are in quite good agreement with observation. Nevertheless, galaxy properties depend also on halo properties other than mass. For example, at given halo mass, more concentrated haloes form earlier and are denser; as a result they form stars more efficiently. Direct estimation of such effects from semi-analytic models can help to understand the scatter in the $M_{\star}-M_{\text{halo}}$ relation.

Together, the MS and the MS-II provide sufficient resolution and statistics to measure the abundance of dark matter subhaloes across seven orders of magnitude in infall mass (Fig. 1). Since this mass function varies very little between WMAP7 and WMAP1, and our galaxy formation parameters are chosen to reproduce the observed stellar mass function in both cases, the relation between stellar mass and infall halo mass barely changes between the two cosmologies. In the upper panel of Fig. 7, error bars are centred on the median value and have length equal to twice the rms scatter in stellar mass for given infall (sub)halo mass and are shown in green for WMAP7 and in red for WMAP1. The ratio of the two median stellar masses is shown in the lower panel. A blue line gives the relation obtained by Guo et al. (2010) for the WMAP1 case when assuming a monotonic scatter-free relation and forcing the stellar mass function to follow the observational data of Fig. 5 exactly. As expected, both simulation results are consistent with the abundance matching relation over the mass range $10^{10} - 10^{14} M_{\odot}/h$. At low mass, galaxies of given stellar mass reside in more massive halos in WMAP7, while at high mass they are hosted by less massive halos. As can be seen from the ratio plot in the lower panel, above a halo mass of about $5 \times 10^{11} M_{\odot}/h$, galaxy formation is more efficient in WMAP7 than in WMAP1, while in lower mass haloes it is the other way around. The effects are very small, however: galaxy masses at fixed halo mass vary by a maximum of about 10%.

3.3 Gas-phase metallicities

Fig. 8 plots gas-phase metallicity against stellar mass for star-forming galaxies, defined to be those with specific star formation rate higher than $10^{-11}/\text{yr}$. The upper panel is for the WMAP7 and the lower panel for WMAP1. In each case black dots are randomly selected simulated galaxies from the MS-II, while the red diamonds represent observational data (Tremonti et al. 2004; Lee et al. 2006). Predictions in both cosmologies agree with the observations reasonably well (the same yields were assumed in the two cases). The median metallicity is about 0.1 dex higher in WMAP7 than in WMAP1, thus closer to the observations, and the scatter is slightly bigger. In neither cosmology does the model reproduce the observed turnover in gas-phase metallicity at the highest masses.

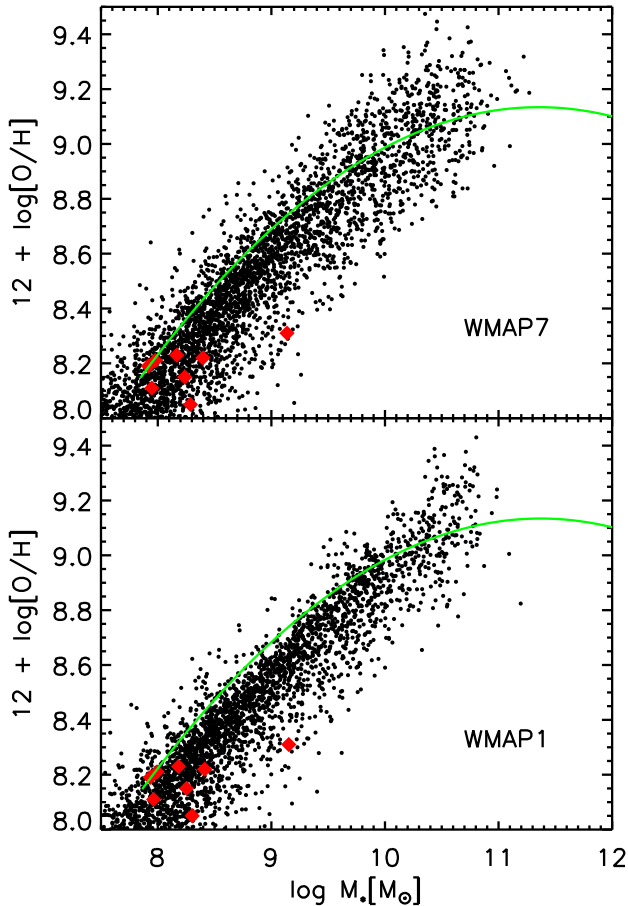


Figure 8. Cold gas metallicity as a function of stellar mass. The top panel shows results for WMAP7, and the bottom panel for WMAP1. In both panels, the solid curves represent observational results for the SDSS from Tremonti et al. (2004), while red diamonds are taken from Lee et al. (2006).

3.4 $u-i$ colour distribution

One of the main problems found by G11 with their WMAP1 model was that it predicts dwarf galaxies that are too red. This may be an indication that dwarfs form too early, and, indeed, at $z > 0.8$ the model substantially overpredicts the abundance of galaxies less massive than a few $10^{10} M_{\odot}$. Structures form somewhat later in the WMAP7 cosmology, so one might expect a delay in the formation of galaxies, leading to a bluer $z = 0$ colour at given stellar mass. Fig. 9 compares model colour distributions for WMAP7 (thick black lines) and WMAP1 (thin black lines) with SDSS data (red dashed lines) as a function of stellar mass. In general, the WMAP7 model does predict slightly bluer galaxies than WMAP1, but the effect is small and the disagreement with the observations remains large, particularly for low-mass galaxies.

In Fig. 10 we investigate this problem further by separating model galaxies into central (blue) and satellite (red) populations. Results for the two cosmologies are almost identical. In both cases, almost all the red population at low stellar mass is contributed by satellites (see also, Weimann et al. 2011). Above about $10^9 M_{\odot}$, the predicted

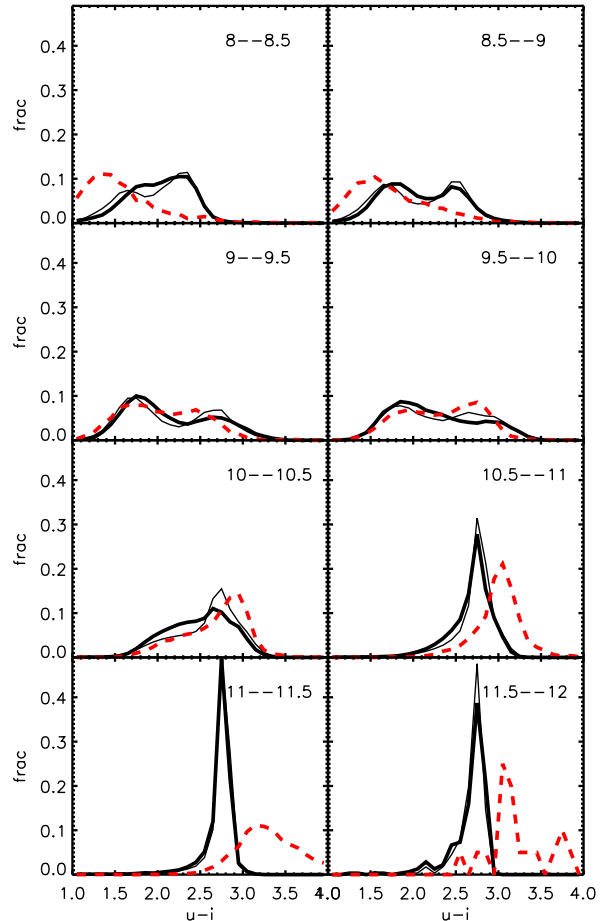


Figure 9. $u-i$ colour distributions as a function of stellar mass. Thick solid black curves show the distributions predicted by our preferred WMAP7 model, while thin curves are for WMAP1. Dashed red curves are distributions compiled from SDSS/DR7.

red fraction is consistent with observation, but at lower masses the models show a peak of red satellites which is missing in the SDSS data. This could either be because too many low-mass galaxies form at high redshift and survive as satellites to the present day, or be because star formation is quenched too efficiently in satellites in the simulations. Another possibility is that the red satellite population has been missed in the SDSS data, perhaps because its surface brightness is too low.

3.5 Cluster number density profiles

G11 showed that their WMAP1 model was able to reproduce the observed mean number density profile of galaxies in rich galaxy clusters between about 30 kpc and 1.5 Mpc both in the MS and in the MS-II. They used this to argue that their treatment of “orphan galaxies” (satellite galaxies for which the corresponding dark matter subhalo had been completely destroyed by tidal effects) was realistic since such galaxies are much less important at the higher resolution of the MS-II. For both simulations they found a projected cluster number density which appeared marginally higher than

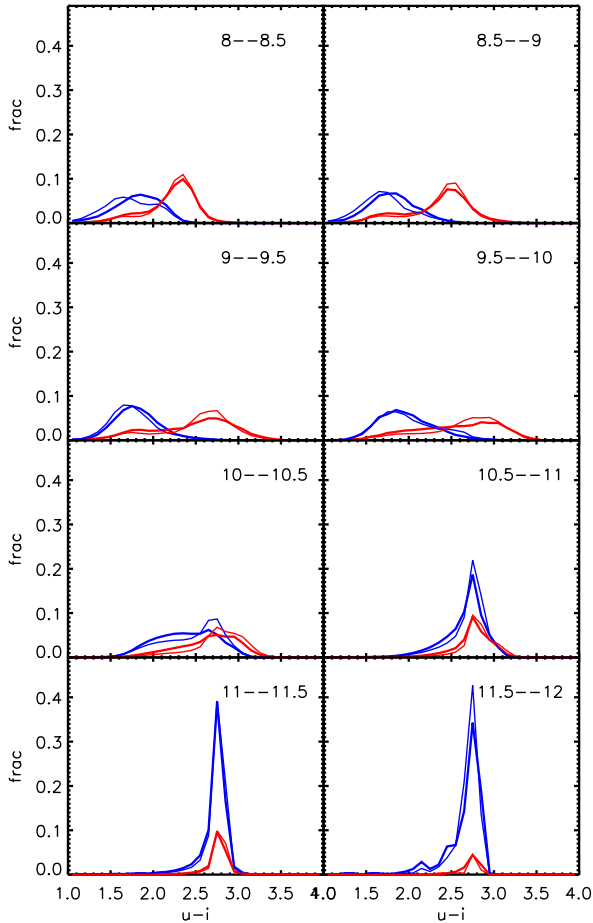


Figure 10. $u-i$ colour distributions as a function of stellar mass for centrals (blue) and satellites (red). Thick curves are results for WMAP7 while thin curves are for WMAP1.

observed below about 150 kpc. Here we revisit this topic, comparing predictions for cluster structure in the WMAP1 and WMAP7 cosmologies.

We follow the procedures in G11 exactly to make this comparison. We use a simple ‘observational’ cluster finder to select galaxy clusters in the same way in the simulations and in the SDSS. Here we summarize the main cluster selection criteria; details are given in G11. Galaxies with mass greater than $6 \times 10^9 h^{-2} M_{\odot}$ are counted around potential BCGs at projected separations $r_p < 1.1 \text{ Mpc}/h$ and redshift differences $|\Delta v| < 1200 \text{ km/s}$. Clusters with counts in the range $45 < N_g < 105$ are accepted. In the MS this leads to a sample of 2295 clusters for the WMAP1 cosmology, and 2443 for WMAP7. G11 estimate the observed number density of clusters defined in this way to be $2 \times 10^{-6} (h/\text{Mpc})^3$, closer to the simulation value for WMAP7 than for WMAP1, although both are probably consistent within the overall uncertainties. The number of clusters in the SDSS spectroscopic database which are complete to this stellar mass limit and satisfy the count criteria is just 31.

Fig.11 compares mean projected number density profiles for stacks of MS clusters in each of the two cosmologies and in the SDSS data. The green curve is for WMAP7, the

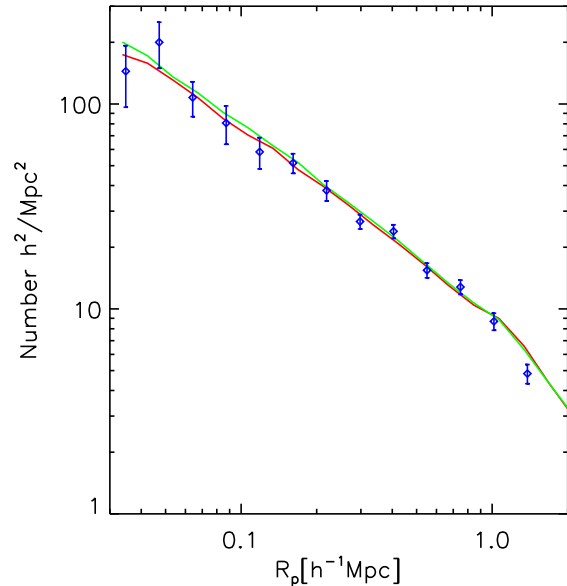


Figure 11. Projected number density profiles for galaxies with stellar mass above $6 \times 10^9 h^{-2} M_{\odot}$ in clusters with $10^{14} M_{\odot} < M_{200} < 2 \times 10^{14} M_{\odot}$. The green curve is the result for WMAP7 while the red curve is for WMAP1. Blue symbols with error bars are from the SDSS (see G11 for further details).

red for WMAP1 and the blue symbols for SDSS, with error bars indicating the *rms* cluster-to-cluster scatter. The overall agreement between simulation and observation is quite good with the model perhaps overproducing galaxies close to cluster center. Results for the two cosmologies are almost identical with WMAP7 (green curve) giving a very slightly higher amplitude, consistent with the higher galaxy formation efficiency for WMAP7 in this mass range (see Fig. 7).

3.6 Correlation Functions

In G11 the parameters of the galaxy formation model were tuned to reproduce the observed abundances of galaxies, particularly their stellar mass functions and the distributions of internal properties like colour, morphology and gas content. The clustering and the evolution of the population were then used as tests of the model. For massive galaxies the observed low-redshift autocorrelation functions were well reproduced from scales of 20 kpc out to $\sim 30 \text{ Mpc}$. For less massive galaxies the agreement remains good on large scales where correlations are due to pairs of galaxies inhabiting different dark matter haloes, but the clustering is noticeably too strong on smaller scales where pairs are predominantly members of the same halo. G11 suggested that this discrepancy might reflect the fact that the overall amplitude of dark matter structure, in particular the parameter σ_8 , is higher in the WMAP1 cosmology than estimated from more recent data.

In Fig. 12 we compare projected two-point correlation functions for our WMAP1 and WMAP7 models to observational data from SDSS/DR7. The observational data here are exactly as in G11, but the WMAP1 model predictions

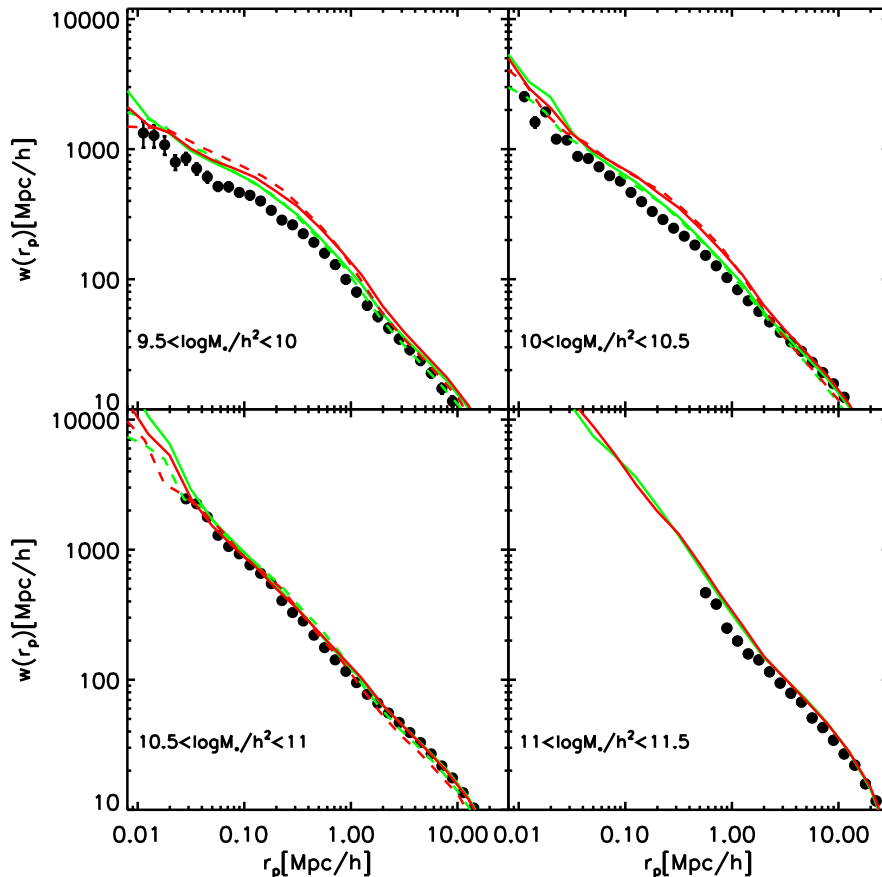


Figure 12. Projected autocorrelation functions for galaxies in different stellar mass ranges. Symbols with error bars are results for SDSS/DR7 calculated using the techniques of Li et al. (2006). Solid and dashed curves give results for our preferred model applied to the MS and the MS-II, respectively. Green curves are for the WMAP7 and red for WMAP1. In general the WMAP7 results are slightly lower than WMAP1, particularly for lower mass galaxies and on small scales where the one-halo term due to satellite galaxies is dominant.

have changed slightly because of the correction of minor software bugs in the galaxy disruption module (see Sec. 2). For each cosmology we show results for both the MS (solid lines) and the MS-II (dashed lines). It is reassuring that the agreement between the two simulations is very good in both cosmologies despite the two orders of magnitude difference in their mass resolution. This gives us confidence that our clustering results are well converged even for low-mass galaxies and on small scales. On large scales and for high-mass galaxies there is almost no difference in clustering between the two cosmologies. However, for pair separations below ~ 1 Mpc and stellar masses below $\sim 10^{10.5} M_{\odot}$, the correlations are clearly weaker for WMAP7 (green) than for WMAP1 (red), although they remain somewhat higher than observed in SDSS. Notice that the difference in large-scale clustering between the two cosmologies is considerably smaller for the galaxies than for the mass. This is because the difference in σ_8 is largely compensated by a difference in bias, which is significantly higher at given stellar mass in WMAP7 than in WMAP1. Note that for the rescaled WMAP7 cosmology, we do not adjust large-scale modes according to the final step of the Angulo & White (2010) procedure. Tests show that this causes only very small changes in MS correlations on

the scales we analyse here, and it has no measurable effect on the MS-II correlations.

3.7 Results at higher redshift

So far we have compared our predictions for galaxy formation in the WMAP1 and WMAP7 cosmologies to low redshift data, using the observed galaxy abundance as a function of stellar mass, luminosity, metallicity and gas content to set our adjustable efficiency parameters, and then searching for dependencies on background cosmology using clustering and colour data. Here we compare predictions for the two models to higher redshift data in order to test whether an updated cosmology can solve the evolutionary problem identified by G11: although their WMAP1 model reproduced the observed cosmic star formation history moderately well and was consistent with the observed abundance of massive galaxies out to $z \sim 4$, it overpredicted the abundance of lower mass galaxies ($M_{\star} < 10^{10.5} M_{\odot}$) at $z \geq 1$. Dwarf galaxies seem to form too early and to age too quickly in this model.

Fig. 13 shows the evolution of the cosmic star formation rate density. The green curve is the mean total star formation rate per unit volume as a function of redshift for our

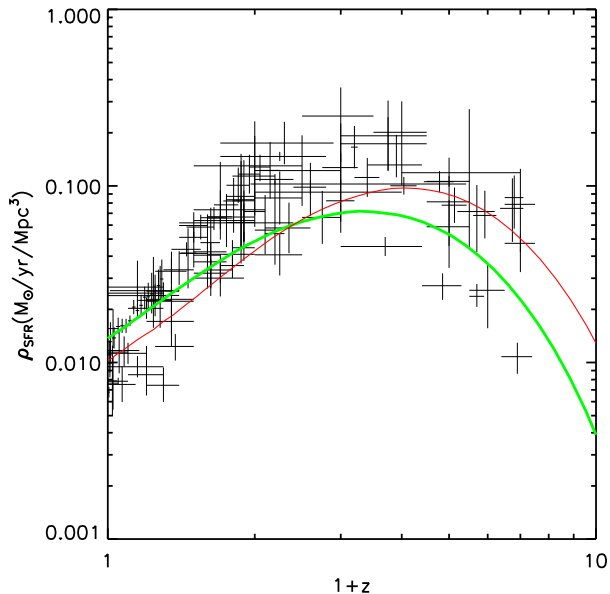


Figure 13. Cosmic star formation rate density as a function of redshift. The crosses are individual observational estimates compiled by Hopkins et al. (2007). The thick solid green curve is obtained from our preferred WMAP7 model whereas the thin red curve is for WMAP1.

WMAP7 model, while the red curve is for WMAP1. The symbols are observational estimates compiled by Hopkins (2007). In both cases, the predictions of the models agree moderately well with the observations. Star formation peaks at significantly lower redshift and the present day star formation rate density is slightly higher in the WMAP7 model than for WMAP1. The first of these shifts improves the agreement with the observational data, while the second makes it worse, particularly after accounting for the normalisation difference caused by the fact that integrating a smooth representation of the observational points in this plot produces a stellar mass density at $z = 0$ which is significantly higher than the value implied by the observed low-redshift stellar mass function used to set our model parameters. The later formation of galaxies in WMAP7 is responsible for the bluer $z = 0$ colours visible in Fig. 9.

In Fig. 14 we investigate how changing cosmology affects the problem of overly early dwarf galaxy formation identified by G11. This plot shows stellar mass functions averaged over four disjoint redshift intervals, as noted in each panel. The observational data are the same as used by G11. The red curves, representing our WMAP1 model, are essentially identical to those in their Fig. 23. It is clear from the green WMAP7 curves that the later formation of structure in the newer cosmology has only a minor effect on these mass functions and does little to reconcile model predictions with observation. This is not surprising given the similar (sub)halo mass functions out to at least $z = 1$ (see Fig. 1). The discrepancy at low mass must reflect a deficiency in the galaxy formation physics, rather than in cosmological parameters. Clearly, star formation at early times must be less efficient in low-mass halos than the current models assume.

This must be compensated by higher efficiencies at later times so that the $z = 0$ stellar mass function is nevertheless reproduced.

As discussed in Sec. 3.2, it is instructive to study the relation between the stellar mass of a galaxy and the maximum past mass of the halo which hosts it. Here we investigate how this relation evolves with redshift in our models. The upper left panel of Fig. 15 shows the mean relation at redshifts 1.0, 1.5 and 2. The colored curves are for our WMAP7 model and are almost coincident with each other, but are shifted noticeably with respect to the $z = 0$ curve of Fig. 7, repeated here as a grey curve. The model relation is almost independent of redshift beyond $z = 1$, although at the highest masses, a slightly lower galaxy formation efficiency is found at earlier times. Wake et al. (2011) use data from the NEWFIRM Medium Band Survey to study the stellar mass vs. halo mass relation within the same redshift intervals. Their results, shown with symbols, are based on fitting a WMAP7 Halo Occupation Distribution model to the abundance and clustering of stellar mass limited samples of galaxies. Since the measured abundances are much more constraining than the clustering, the information content of these points is very similar to that of the stellar mass function of Fig. 14. Wake et al. (2011) found no significant change in their HOD parameters over $1 < z < 2$ but a noticeable shift from $z = 0$. The first result is directly visible in Fig. 15, while the second is responsible for the steepness of the observed relation over the limited stellar mass range for which it can be estimated, reflecting the lowered amplitude of the stellar mass function below its characteristic mass which is seen in the data but not in our models (see Fig. 14).

The cosmology dependence of this relation is illustrated in the bottom left panel of Fig. 15 which, for galaxies of given maximum past halo mass, gives the ratio of mean stellar mass in the WMAP7 and WMAP1 models. Galaxy formation efficiencies are similar in the two models at all redshifts shown. There is a characteristic halo mass around $10^{12} M_{\odot}/h$ where the formation efficiency switches from being higher in WMAP1 to being higher in WMAP7. This mass is closely related to that where galaxy formation efficiency peaks (e.g. Guo et al. 2010) and is higher (and almost constant) for $1 \lesssim z \lesssim 2$ than for $z = 0$. This shift reflects the “halo downsizing” pointed out by Wake et al. (2011). Overall, however, only minor differences in galaxy formation efficiency are expected between our two cosmologies at these redshifts.

The upper right panel of Fig. 15 shows the scatter in central galaxy stellar mass as a function of maximum past halo mass for our WMAP7 model. This scatter increases slightly for halo masses between $10^{9.5} M_{\odot}/h$ and $10^{11} M_{\odot}/h$, reaching a maximum of ~ 0.35 dex before dropping rapidly to 0.2 dex at masses above $2 \times 10^{12} M_{\odot}/h$. Again, the scatter does not depend on redshift and is similar to that at $z = 0$. Notice that it is larger than the differences between the “observed” and predicted mean relations in the upper left panel. Finally, the lower right panel shows how the predicted scatter changes between our two cosmologies. Here too differences are small. Below $10^{12} M_{\odot}/h$ and also at the highest masses the scatter is higher for WMAP7.

We finish this section by studying the sensitivity of high-redshift galaxy clustering to background cosmology. In Fig. 16 we show projected correlation functions for three of

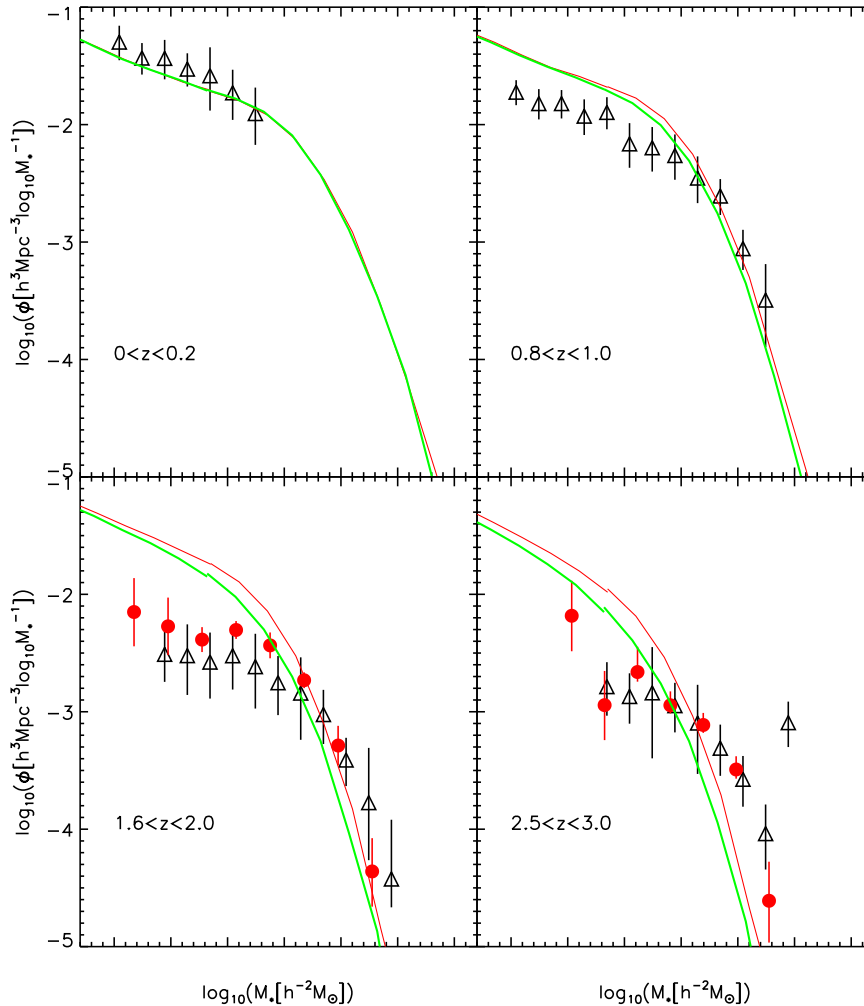


Figure 14. Stellar mass functions for a series of redshift intervals indicated by the labels in each panel. Observational data are taken from Perez-Gonzalez et al. (2008) and from Marchesini et al. (2009). The mass scales of these observational results have been shifted to correct approximately to the Chabrier IMF assumed in our modelling. Solid curves are the functions measured from the combination of the MS and the MS-II for our preferred galaxy formation model, convolving with a Gaussian of dispersion 0.25 dex in $\log M_*$ to represent the uncertainty in observational estimates of M_* . Green curves are for our WMAP7 model, while red curves are for WMAP1.

the stellar mass bins of Fig. 12 and for redshifts 0, 1 and 3. Red curves are for WMAP1 and green for WMAP7. We have multiplied these functions by r_p in order to make differences more visible (compare the $z = 0$ curves in Figs 12 and 16). In the local universe, correlations are predicted to be weaker in WMAP7 than in WMAP1 for stellar masses below $10^{10.5} M_\odot$, and to be very similar at higher mass. By redshift 1 the predicted correlation amplitude in WMAP7 has increased substantially relative to WMAP1. The two now coincide for $M_* < 10^{10.5} M_\odot$ and WMAP7 is more clustered at higher stellar mass. This trend increases with increasing redshift so that by $z = 3$ the WMAP7 model predicts larger clustering amplitudes than WMAP1 at all stellar masses. Thus although the dark matter is substantially less clustered at high redshift for the more recent cosmological parameters (see Fig. 1), bias effects cause the opposite to be true for galaxies of any given stellar mass. The differences are nevertheless quite small over this redshift range,

and current data are insufficiently precise to distinguish the two cosmologies.

4 CONCLUSION

We have used the re-scaling technique recently developed by Angulo & White (2010) to scale the Millennium and Millennium-II simulations from the WMAP1 cosmology in which they were carried out to the currently favoured WMAP7 cosmology. The amplitude parameter σ_8 is lower but the matter density Ω_m is higher for WMAP7 than for WMAP1. These two changes have partially compensating effects, producing halo mass functions which are similar in the two cosmologies out to redshifts of at least 3. As a result, a slightly updated version of the galaxy formation model of Guo et al. (2011) produces equally good fits to low-redshift data in the two cases with only minor adjustments of its

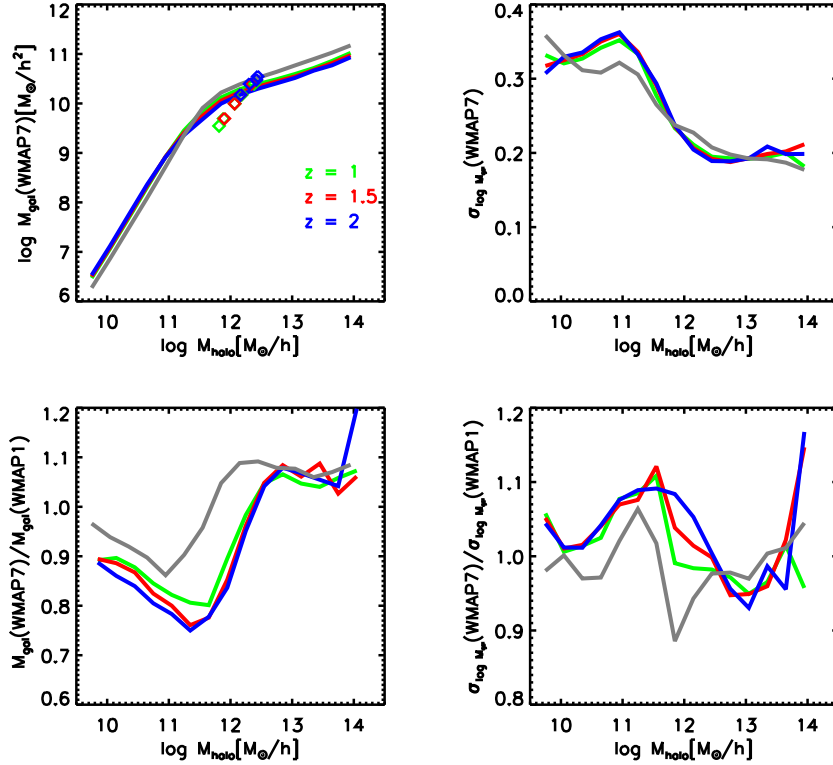


Figure 15. Upper left panel: galaxy stellar mass as a function of maximum past halo mass at various redshifts for our WMAP7 galaxy formation model. Symbols are observational estimates by Wake et al. (2011) based on fits of an HOD model to abundance and clustering data *assuming* this cosmology. Different colours refer to different redshifts as indicated in the bottom right corner. The curves almost coincide and are also very close to the $z = 0$ curve shown in Fig. 7. Bottom left panel: the ratio of galaxy stellar mass for WMAP7 to that for WMAP1 as a function of halo mass and at various redshifts. Lines are colour coded as in the upper left panel. Upper right panel: one sigma scatter in galaxy stellar mass as a function of halo mass. Again, the solid curve is for our WMAP7 model while symbols show the deviation of observational points of Wake et al.(2011) from our WMAP7 model. Right bottom panel: ratio of the one sigma scatter in stellar mass between WMAP7 and WMAP1 as a function of halo mass.

Table 2. Summary of those parameters of our preferred model which were adjusted to fit low-redshift observational data, primarily the stellar mass function.

| Parameter | Description | WMAP1 | WMAP7 |
|--------------|---|----------------------|--------------------|
| α | Star formation efficiency | 0.02 | 0.011 |
| ϵ | Amplitude of SN reheating efficiency | 6.5 | 4 |
| β_1 | Slope of SN reheating efficiency | 3.5 | 3.2 |
| V_{reheat} | normalization of SN reheating efficiency dependence on Vmax | 70 | 80 |
| η | Amplitude of SN ejection efficiency | 0.32 | 0.18 |
| β_2 | Slope of SN ejection efficiency | 3.5 | 3.2 |
| V_{eject} | normalization of SN ejection efficiency dependence on Vmax | 70 | 90 |
| κ | Hot gas accretion efficiency onto black holes | 1.5×10^{-5} | 7×10^{-6} |

parameters. Furthermore, the predicted evolution since redshift 3 is also quite similar, although some residual cosmological dependencies remain, particularly in the clustering properties.

The main parameters affecting the stellar mass function are the efficiencies of star formation, of SN and AGN feedback, and of reincorporation of ejected material. In general, we require lower star-formation efficiency and weaker feedback in WMAP7 than in WMAP1 in order to produce a similar $z = 0$ galaxy population. As a result, the cosmic

star-formation rate peaks later in WMAP7 than in WMAP1, and galaxies are bluer at low redshift. For halos more massive than $10^{11.5} M_{\odot}$, galaxy formation is more efficient in WMAP7 than in WMAP1, while the reverse is true for lower mass haloes. The predicted two-point correlations of low-mass galaxies agree better with observation for WMAP7 than for WMAP1, although their amplitude on small scales is still slightly higher than observed. The overly early formation of such galaxies noted by Guo et al. (2011) (see also Henriques et al. (2012)) is scarcely affected by the shift to a

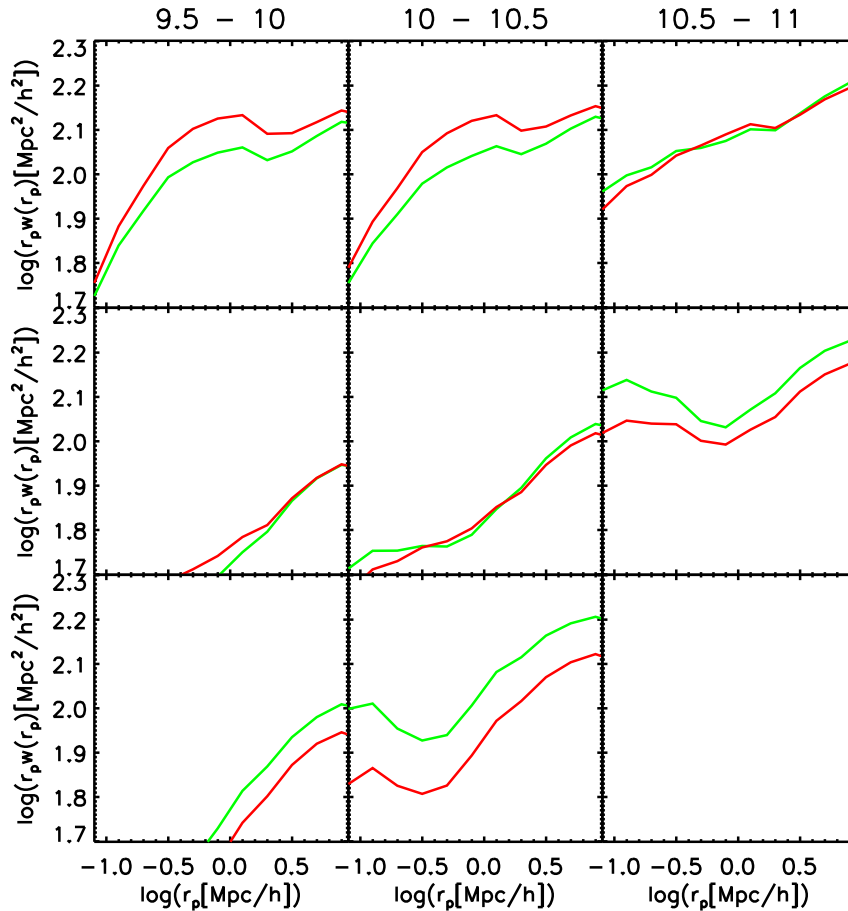


Figure 16. Projected correlation functions (multiplied by r_p as a function of redshift and stellar mass for our two cosmologies. Red curves refer to WMAP1 and green to WMAP7.

WMAP7 cosmology. Clearly, observations require the galaxy formation efficiency to be lowered in low-mass haloes at early times, and then increased at late times to produce a similar $z = 0$ galaxy population.

Our results contrast with those of Wang et al. (2008) who compared galaxy properties in simulations of the WMAP1 and WMAP3 cosmologies. For similar $z = 0$ galaxy populations, they found the abundance and clustering of high-redshift galaxies to differ substantially between the two cosmologies. This reflects the fact that their WMAP3 model assumed $\sigma_8 = 0.72$ and $\Omega_m = 0.226$, both significantly lower than in our WMAP7 cosmology. Indeed, their Ω_m value is even lower than the one we assume for WMAP1. As a result, the differences in halo mass function between their two cosmologies are much larger than between our WMAP1 and WMAP7 models. Recent work by Kang et al. (2012) also finds very little variation of galaxy clustering between the WMAP1 and WMAP7 cosmologies.

In summary, with the WMAP7 cosmological parameters adopted here, we find only small differences in galaxy properties relative to the WMAP1 model of G11, both in the local universe and at high redshift. This is a consequence of the similar mass functions predicted by these two cosmologies over the range of redshifts where galaxies form most of their stars. The difference in cosmology is, in effect, too small to show up strongly in either the evolution or the clustering

of the galaxies. Given the substantial residual uncertainties in galaxy formation modelling, it is not currently possible to distinguish the two cosmologies using properties of the galaxy population. This may reflect a degeneracy in the larger space of cosmological and galaxy formation parameters. Our galaxy formation and simulation scaling techniques make it feasible to combine low- and high-redshift clustering and abundance data to constrain this larger parameter space, and may eventually make it possible to separate information about galaxy formation processes from information about the larger cosmological context in which they take place.

ACKNOWLEDGEMENTS

Galaxy, halo and lightcone catalogues corresponding closely to the WMAP1 models of this paper are publicly available at <http://www.mpa-garching.mpg.de/millennium> and similar catalogues for the WMAP7 model will be made available on the same site as soon as this paper is accepted for publication. REA, BH, GL and SW are supported by Advanced Grant 246797 GALFORMOD from the European Research Council. GQ acknowledges support from the National basic research program of China (program 973 under grant No. 2009CB24901), the Young Researcher Grant of National

Astronomical Observatories, CAS, the NSFC grants program (No. 11143005) and the Partner Group program of the Max Planck Society. MB-K acknowledges support from the Southern California Center for Galaxy Evolution, a multi-campus research program funded by the University of California Office of Research.

REFERENCES

- Angulo R. E., White S. D. M., 2010, *MNRAS*, 405, 143
- Baldry I. K., Glazebrook K., Driver S. P., 2008, *MNRAS*, 388, 945
- Bigiel F., Leroy A. K., Walter F., Brinks E., de Blok W. J. G., Kramer C., Rix H. W., Schrubba A., Schuster K.-F., Usero A., Wiesemeyer H. W., 2011, *ApJ*, 730, L13
- Boylan-Kolchin M., Springel V., White S. D. M., Jenkins A., Lemson G., 2009, *MNRAS*, 398, 1150
- Conroy C., Wechsler R. H., Kravtsov A. V., 2006, *ApJ*, 647, 201
- Croton D. J., Springel V., White S. D. M., De Lucia G., Frenk C. S., Gao L., Jenkins A., Kauffmann G., Navarro J. F., Yoshida N., 2006, *MNRAS*, 365, 11
- De Lucia G., Blaizot J., 2007, *MNRAS*, 375, 2
- Gao L., De Lucia G., White S. D. M., Jenkins A., 2004, *MNRAS*, 352, L1
- Guo Q., White S., Boylan-Kolchin M., De Lucia G., Kauffmann G., Lemson G., Li C., Springel V., Weinmann S., 2011, *MNRAS*, 413, 101
- Guo Q., White S., Li C., Boylan-Kolchin M., 2010, *MNRAS*, 404, 1111
- Henriques B. M. B., White S. D. M., Lemson G., Thomas P. A., Guo Q., Marleau G.-D., Overzier R. A., 2012, *MNRAS*, 421, 2904
- Hopkins A. M., 2007, in Afonso J., Ferguson H. C., Mobasher B., Norris R., eds, *Deepest Astronomical Surveys Vol. 380 of Astronomical Society of the Pacific Conference Series, The Star Formation History of the Universe*. p. 423
- Kang X., Li M., Lin W. P., Elahi P. J., 2012, *MNRAS*, 422, 804
- Kauffmann G., Colberg J. M., Diaferio A., White S. D. M., 1999, *MNRAS*, 303, 188
- Komatsu E., Smith K. M., Dunkley J., Bennett C. L., Gold B., Hinshaw G., Jarosik N., Larson D., et al. 2011, *ApJS*, 192, 18
- Lee H., Skillman E. D., Cannon J. M., Jackson D. C., Gehrz R. D., Polomski E. F., Woodward C. E., 2006, *ApJ*, 647, 970
- Li C., White S. D. M., 2009, *MNRAS*, 398, 2177
- Moster B. P., Somerville R. S., Maubetsch C., van den Bosch F. C., Macciò A. V., Naab T., Oser L., 2010, *ApJ*, 710, 903
- Rees M. J., Ostriker J. P., 1977, *MNRAS*, 179, 541
- Ruiz A. N., Padilla N. D., Domínguez M. J., Cora S. A., 2011, *MNRAS*, 418, 2422
- Smith R. E., 2012, *ArXiv e-prints*
- Springel V., White S. D. M., Jenkins A., Frenk C. S., Yoshida N., Gao L., Navarro J., Thacker R., et al. 2005, *Nature*, 435, 629
- Springel V., White S. D. M., Tormen G., Kauffmann G., 2001, *MNRAS*, 328, 726
- Tremonti C. A., Heckman T. M., Kauffmann G., Brinchmann J., Charlot S., White S. D. M., Seibert M., Peng E. W., Schlegel D. J., Uomoto A., Fukugita M., Brinkmann J., 2004, *ApJ*, 613, 898
- Vale A., Ostriker J. P., 2004, *MNRAS*, 353, 189
- van de Voort F., Schaye J., Booth C. M., Dalla Vecchia C., 2011, *MNRAS*, 415, 2782
- Wake D. A., Whitaker K. E., Labbé I., van Dokkum P. G., Franx M., Quadri R., Brammer G., Kriek M., Lundgren B. F., Marchesini D., Muzzin A., 2011, *ApJ*, 728, 46
- Wang J., De Lucia G., Kitzbichler M. G., White S. D. M., 2008, *MNRAS*, 384, 1301
- Weinmann S. M., Lisker T., Guo Q., Meyer H. T., Janz J., 2011, *MNRAS*, 416, 1197
- White S. D. M., Frenk C. S., 1991, *ApJ*, 379, 52
- White S. D. M., Rees M. J., 1978, *MNRAS*, 183, 341